Thin Solid Films 544 (2013) 580–587

Contents lists available at ScienceDirect

Thin Solid Films

journal homepage: www.elsevier.com/locate/tsf

Oxidation resistance and structural evolution of (TiVCrZrHf)N coatings

Du-Cheng Tsai [a], Zue-Chin Chang [b], Li-Yu Kuo [a], Tien-Jen Lin [a], Tai-Nan Lin [c], Ming-Hua Shiao [d], Fuh-Sheng Shieu [a,*]

[a] Department of Materials Science and Engineering, National Chung Hsing University, Taichung 40227, Taiwan
[b] Department of Mechanical Engineering, National Chin-Yi University of Technology, Taichung 41170, Taiwan
[c] Chemical Engineering Division, Institute of Nuclear Energy Research, Taoyuan County, 32546, Taiwan
[d] Instrument Technology Research Center, National Applied Research Laboratories, Hsinchu, 300, Taiwan

ARTICLE INFO

Available online 3 January 2013

Keywords:
Coating materials
Nitride materials
Vapor deposition
Crystal structure
Transmission electron microscopy
TEM

ABSTRACT

(TiVCrZrHf)N coatings were deposited on Si substrates by reactive magnetron sputtering system. Their oxidation behaviors and structure were studied after static oxidation tests in air at different temperatures. The evolution of the chemical composition, microstructure, nanohardness, and electrical resistivity of these coatings after annealing at different temperatures in air was systematically analyzed. The as-deposited coating showed continued variation in structure from amorphous to columnar with the face-centered cubic crystal phase, but had no significant change in structure with increased annealing temperature to 300 °C. The hardness of the coating was stable at a high value of 31.24 GPa up to an annealing temperature of 300 °C. However, a thin oxide overlayer was observed at 400 °C, which increased in thickness at 500 °C and thus drastically decreasing the hardness to 11.85 GPa. Above 600 °C, the coating was almost fully oxidized and became quite porous and loose. Accordingly, a very low hardness of only 2.3 GPa was obtained. The electrical resistivity of the coatings followed the same trend as the hardness. The electrical resistivity of the as-deposited coating was about 144 μΩ-cm, followed by an apparent increase to 100 Ω-cm due to the formation of oxide phases.

1. Introduction

Transition metal nitrides are widely applied as hard protective coatings. Simple binary and ternary nitride systems such as TiN and CrN are commonly used in tools for cutting and forming, machinery components, and aerospace and automotive parts, among others due to their high hardness, wear resistance, thermal stability, oxidation resistance, and chemical stability [1–4]. However, to enhance the performance of particular tools, dies, and molds for several applications, more protective coatings have been intensively investigated, including those with ternary components such as Ti–Cr–N [5,6], Cr–V–N [7], and Ti–V–N [8]; multilayer structure such as TiN/VN [9] and TiN/NbN [10]; and nanocomposite structure such as nc-TiN/a-Si_3N_4 [11] and nc-TiN/a-BN [12].

Recently, high-entropy alloys (HEAs), which are defined as alloys comprising at least five principal elements with concentrations between 5 at.% and 35 at.%, have been proposed and investigated by Yeh et al. [13,14]. The high-entropy, sluggish diffusion, lattice distortion, and cocktail effect resulting from their multi-principal-element mixtures are found to be the core factors influencing the microstructure and properties of the alloys. High mixing entropy enhances mutual solubility among elements and prevents phase separation into ordered phases or intermetallic compounds. The sluggish diffusion of atoms lowers the phase transformation rate and enhances nanoprecipitation as well as nanocrystalline or even amorphous structures. The distorted lattice is exploited to promote the mechanical, physical, and chemical properties of the alloys. Finally, cocktail effects result in a composite effect on the alloy properties, wherein the interactions among the different elements provides an additional impact apart from the rule of mixtures. With proper alloy designs, HEAs have been found to exhibit versatile properties such as high hardness and superior resistance to temper softening, wear, oxidation, and corrosion. Hence, alloys have great potential applications in tools, molds, dies, and mechanical parts, etc. Previous research on $Al_xCoCrCuFeNi$ [15], $Al_x(TiVCrMnFeCoNiCu)_{100-x}$ [16], and $Al_{0.5}CoCrCuFeNiV_x$ [17,18] alloys reveal their simple body-centered cubic or face-centered cubic (fcc) crystal solid solution structures or the mixture of both, as well as promising mechanical properties, including excellent elevated-temperature strength and good wear resistance.

The coating technology has further expanded the applications of HEAs in functional thin films. Several types of HEA nitride (HEAN) coating, such as TiVCrZrY [19], TiVCrZrHf [20–22], AlCrTaTiZr [23], and AlCrNbSiTiV [24], have been prepared and characterized by sputtering an alloyed target formed by the arc melting process. Metallic coatings and most nitride coatings have amorphous and fcc solid solution structures, respectively. The hardness of these alloy coatings range from 6.8 GPa to 13 GPa, whereas that of the nitrides range from 16 GPa to 48 GPa. Thus, HEANs have great potential use as protective coatings.

In the current study, a TiVCrZrHf target with five strong nitride-forming elements was designed to deposit strong nitride coatings by

* Corresponding author. Tel.: +886 4 2284 0500; fax: +886 4 2285 7017.
E-mail address: fsshieu@dragon.nchu.edu.tw (F.-S. Shieu).

0040-6090/$ – see front matter © 2013 Elsevier B.V. All rights reserved.
http://dx.doi.org/10.1016/j.tsf.2012.12.064

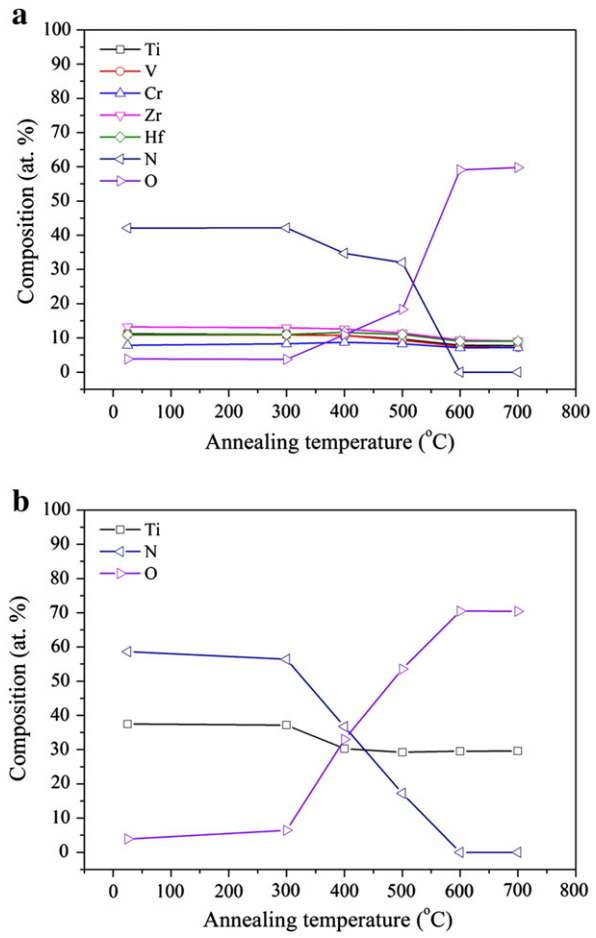

Fig. 1. FE-EPMA elemental content of the (a) (TiVCrZrHf)N and (b) TiN coatings after annealing at different temperatures in air.

reactive radio frequency (RF) magnetron reactive sputtering. Previous works have shown that (TiVCrZrHf)N coatings have superior mechanical properties and high thermal stability [20–22,25]. However, their oxidation resistance and structural changes during a thermal process in air have not yet been systematically investigated. Therefore, this study aimed to explore the oxidation behavior and structural evolution of these coatings. Microstructural observation, compositional determination, as well as mechanical and electrical measurements after annealing the (TiVCrZrHf)N coatings at different temperatures in air were performed.

2. Experiment

The (TiVCrZrHf)N coatings were deposited on p-Si (100) wafers by a reactive RF magnetron sputtering system using equimolar TiVCrZrHf targets (75 mm in diameter). Before deposition, the Si substrates were cleaned and rinsed with ethanol and distilled water in an ultrasonic bath. Then, 1.4 μm-thick (TiVCrZrHf)N coatings were deposited at a plasma power of 350 W and a substrate bias of −100 V in an $Ar+N_2$ mixed atmosphere under a working pressure of 6.67×10^{-1} Pa at 450 °C. The flow rates of Ar and N_2 were maintained at 100 and 4 sccm, respectively. To determine the oxidation resistance of the

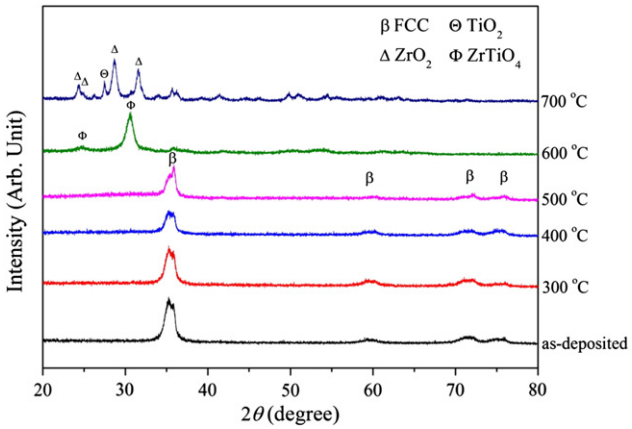

Fig. 2. X-ray diffraction pattern of the (TiVCrZrHf)N coatings after annealing at different temperatures in air.

as-deposited (TiVCrZrHf)N coatings, they were annealed at different temperatures (300–700 °C) for 2 h in air using a furnace.

Variations in the coating composition, structure, as well as mechanical and electrical properties as a function of the annealing temperature were systematically analyzed. The chemical composition of the (TiVCrZrHf)N coatings were determined using a field-emission electron probe microanalysis (FE-EPMA) system (JOEL JXA-8800M). At least three tests were performed for each sample. The crystal structures were analyzed by X-ray diffractometry (XRD, BRUKER D8 Discover) equipment using Cu Kα radiation at a scanning speed of 1°/min. The scanning step was 0.01° and the scanning range was 20° to 80°. Morphological studies and thickness measurements were carried out using a field emission scanning electron microscopy (SEM, JEOL JSM-6700F) system at an acceleration voltage of 3 kV. Microstructure and local composition were investigated by field emission transmission electron microscopy (TEM, FEI E.O. TecnaiF20) equipped with energy-dispersive spectroscopy (EDS) at an acceleration voltage of 200 kV. Cross-sectioned TEM samples were prepared using the focus ion beam (FIB, SMI 3050) lift-out method. Firstly, a protective layer of carbon was deposited over the area of interest using the ion-assisted deposition facility in the FIB. The finely focused Ga+ ion beam was then used to cut electron transparent membranes from the samples. An ex-situ workstation consisting of a fine glass probe, a micromanipulator and a long working distance optical microscope was used to transfer the membranes to a carbon support film on a copper TEM grid. The nanohardness and elastic modulus of the coatings were measured using a TriboLab nanoindenter (Hysitron). At least five replicate tests were performed for each sample. The electrical resistivity of the coatings was measured using a four-point probe system.

3. Results and discussion

Fig. 1a and b shows the plot of the FE-EPMA elemental content of the TiN and (TiVCrZrHf)N coatings after annealing at different temperatures in air, respectively. For (TiVCrZrHf)N coatings, the contents of the five metallic elements in all coatings were in near-equimolar ratios and close to the designed value. Variations in the nitrogen and oxygen contents of the coatings after annealing at different temperatures in air were clearly present. The nitrogen content decreased

Table 1
The enthalpies of formation (Δ*H*) of the five binary nitrides and oxides based on the target elements.

	TiN	TiO_2	VN	V_2O_5	CrN	Cr_2O_3	ZrN	ZrO_2	HfN	HfO_2
ΔH (kJ/per mole of metal element)	−337.7	−944.0	−217.2	−775.0	−117.2	−570.0	−365.3	−1100.6	−373.6	−1144.7

Table 2
Theoretically interplanar spacing (d) and diffraction angle (2θ) of FCC (111) planes of individual nitrides and a mixed (TiVCrZrHf)N coating.

Nitride crystal structure	TiN	VN	CrN	ZrN	HfN	(TiVCrZrHf)N
	FCC	FCC	FCC	FCC	FCC	FCC
d (Å)	2.45	2.39	2.39	2.64	2.61	2.51
2θ (degree)	36.66	37.61	37.60	33.92	34.30	35.84

d and 2θ of mixed (TiVCrZrHf)N: average values based on the rule of mixtures.

Table 3
Binary oxide structure of the present constituent metal element.

Oxide	Lattice parameter (Å)	Crystal structure
TiO_2	a: 4.59, c: 2.95	Tetragonal
V_2O_5	a:11.52, b: 3.57, c: 4.37	Orthorhombic
Cr_2O_3	a: 4.96, c: 13.59	Rhombohedral
ZrO_2	a:5.31, b: 5.21, c: 5.15	Monoclinic
HfO_2	a:5.29, b: 5.18, c: 5.11	Monoclinic

and the oxygen content increased with increased annealing temperature. The coatings started to oxidize at 400 °C, with about 11 at.% oxygen detected. After annealing at 600 °C, no nitrogen was detected, implying complete oxidation. This phenomenon can be attributed to the significantly larger enthalpies of formation of the metal oxides than the corresponding metal nitrides, as listed in Table 1 [26,27]. Therefore, oxygen had a considerable tendency to react with (TiVCrZrHf)N coatings compared with nitrogen. The elemental content of TiN coatings basically followed the same trend as that of (TiVCrZrHf)N coatings.

Fig. 2 shows the XRD patterns of the (TiVCrZrHf)N coatings after annealing at different temperatures in air. According to the Bragg law and the interplanar spacing (d) relation, the as-deposited (TiVCrZrHf)N coating was crystallized in the fcc crystal structure. The (111) peak position of the as-deposited (TiVCrZrHf)N coating was measured at about 35.38°, and the (111) interplanar spacing was calculated as 2.53 Å which just matched the average value of mixed TiN, VN, CrN, ZrN, and HfN as shown in Table 2. This finding not only implied the formation of a solid solution from all constituted nitrides, but also confirmed the effect of a high mixing entropy on the simplification of the crystal structure. Accordingly, the fcc solid structure was expected because each binary nitride of the metallic

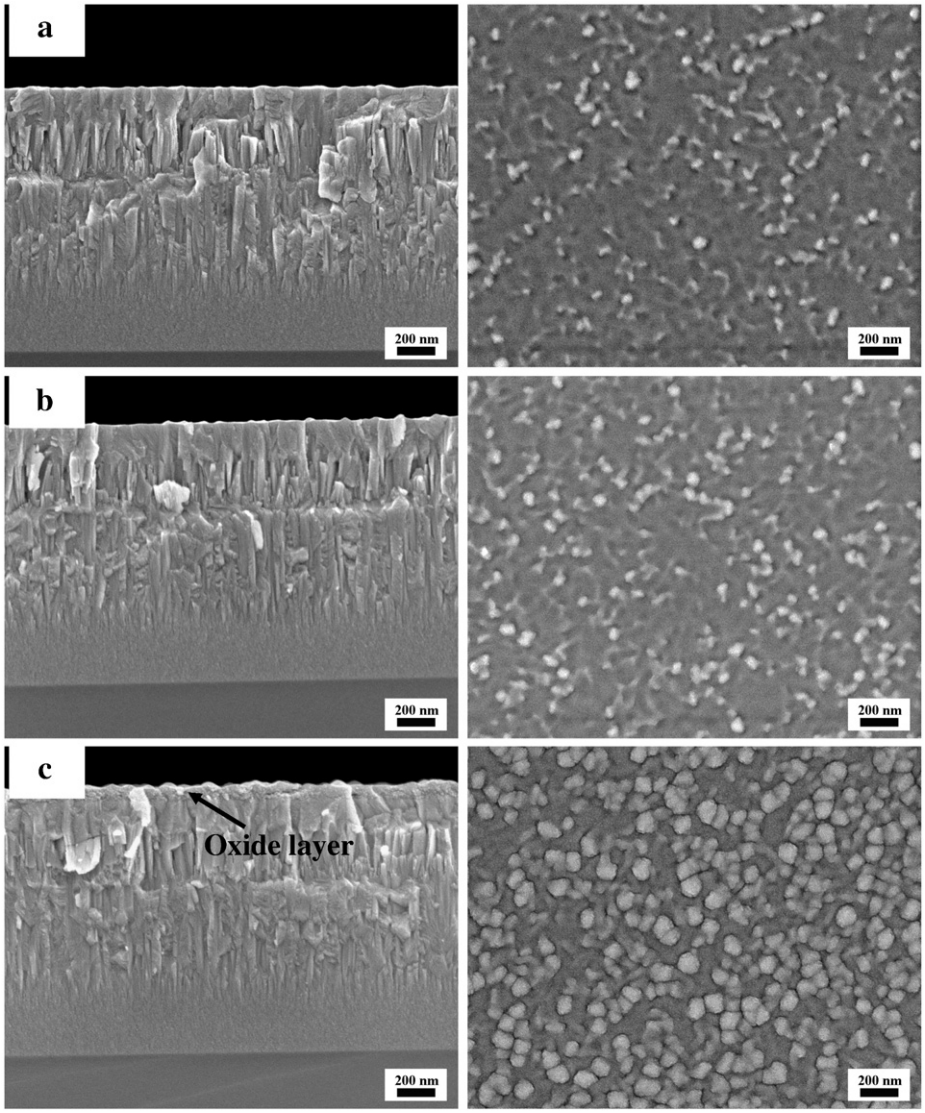

Fig. 3. Plan-view and cross-sectional SEM micrographs of the (TiVCrZrHf)N coatings after annealing at different temperatures in air.: (a) RT, (b) 300, (c) 400, (d) 500, (e) 600, and (f) 700 °C.

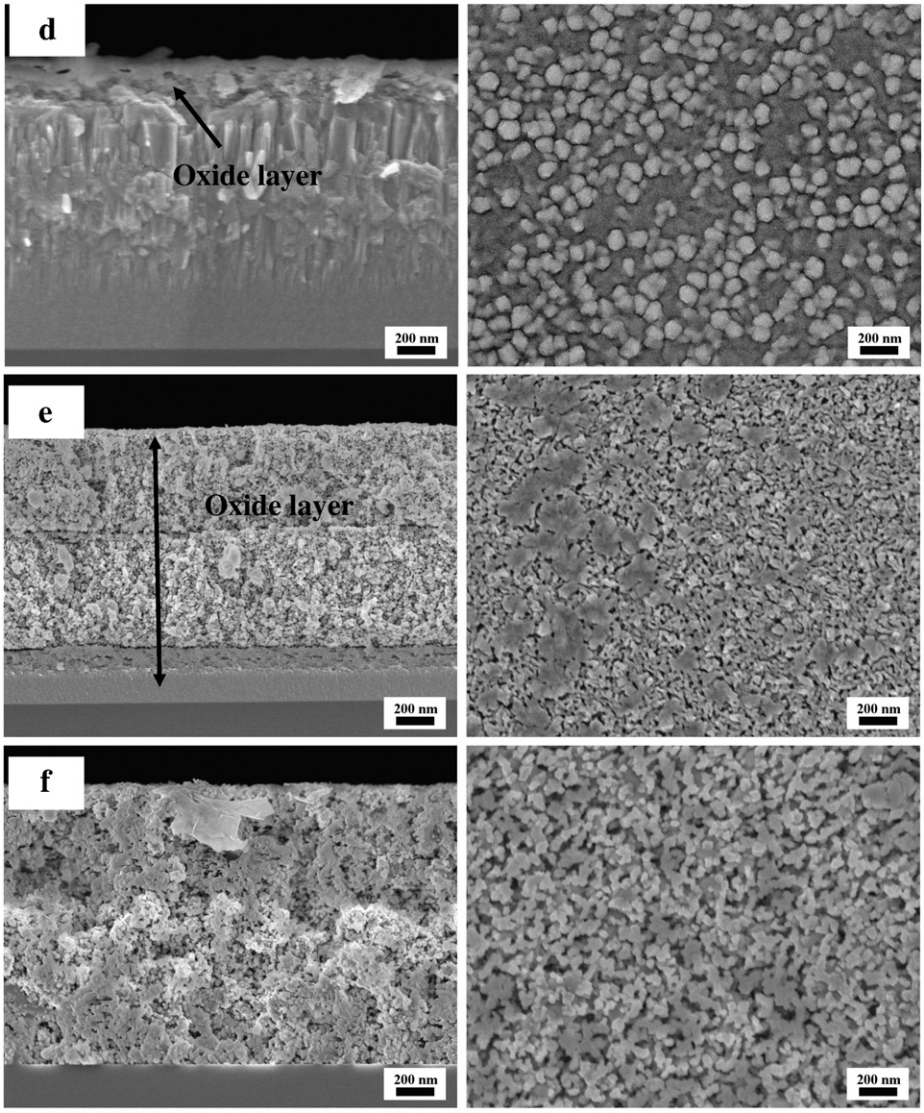

Fig. 3 (*continued*).

constituents formed fcc structures. Similar observations have been reported on TiVCr and AlCrTaTiZr nitride coating systems [23,28].

No other evident oxide peak was detected even when the annealing temperature was increased to 500 °C, although the coating contained 18 at.% O. Such O content or insufficient annealing temperature failed to build the crystal structure of the oxides. However, after annealing at 600 °C, the coating was fully oxidized and the (011) and (111) peaks of the hexagonal $ZrTiO_4$ phase were observed. The intensities of the (111) peak were very high, indicating the existence of highly (111)-oriented $ZrTiO_4$ on the substrates. Kim et al. [29] have obtained (111)-oriented $ZrTiO_4$ films. The atoms arranged according to the preferred orientation tend to reduce their free energy to reach a stable state. With further increased annealing temperature to 700 °C, monoclinic ZrO_2 and rutile TiO_2 formed. $ZrTiO_4$ has been found by Reddy et al. [30] to be thermally stable up to 1000 °C in the absence of any additive atom, but becomes less thermally stable with the addition of other elements. Noguchi and Mizuno [31] have reported that tetragonal and monoclinic ZrO_2 and rutile TiO_2 can be formed by the decomposition of $ZrTiO_4$ compound at higher temperatures. Wu et al. [32] have also reported the formation of the rutile TiO_2 phase at high calcination temperatures. The mechanical stress of cold pressing $ZrTiO_4$ at 147 MPa induces the partial decomposition of $ZrTiO_4$ to monoclinic ZrO_2 at temperatures as low as 300 °C [33]. Accordingly, the instability of $ZrTiO_4$ at 700 °C is expected. The oxidation behavior of (TiVCrZrHf)N coating can be explained by Tables 1 and 3. The driving forces from nitride to oxide are different for different elements. Based on this, TiN, ZrN, and HfN thus have the relatively strong tendency for oxidation. That means, some elements tend to form oxides first such as $ZrTiO_4$, ZrO_2, TiO_2 in the present case. Since Hf and Zr are chemically quite similar and have nearly the same atomic size, there would have some mixing in ZrO_2 and $ZrTiO_4$.

Fig. 3 shows the SEM micrographs of the (TiVCrZrHf)N coatings after annealing at different temperatures in air. The deposition rate is about 15.5 nm/min. The plane-view image shows a very dense and smooth surface morphology, which can be attributed to the application of substrate bias and heating. The cross-sectional image shows two distinct layers separated by a boundary. The underlayer had a smooth morphology without any special feature, whereas the upper layer had a typical columnar structure with a dense and smooth surface. To discuss further the mechanism behind the growth of (TiVCrZrHf)N on Si substrate, subsequent TEM characterizations were performed. Fig. 4a and b illustrates the bright-field and dark-field images, respectively, using the (111) and (200) diffraction rings (circles) in the selected area electron diffraction (SAED) pattern.

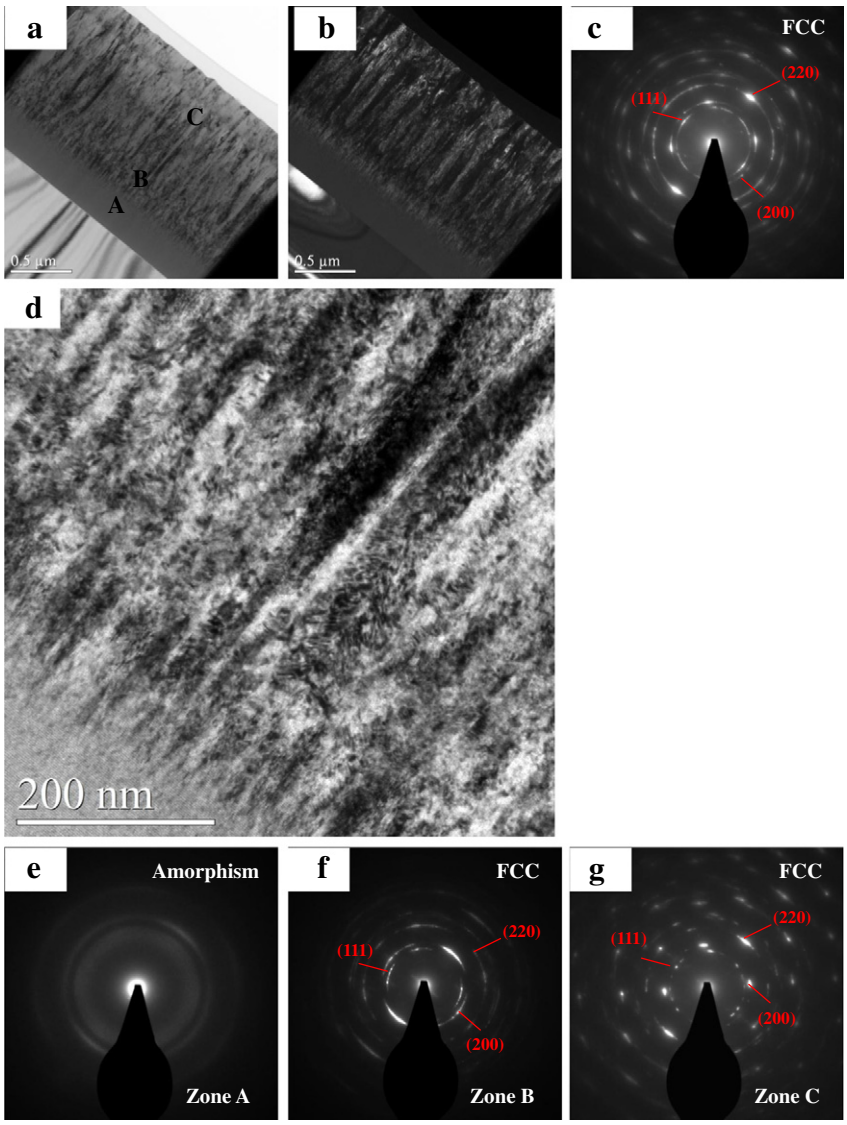

Fig. 4. Cross-sectional TEM micrographs of the as-deposited (TiVCrZrHf)N coatings. (a) Bright-field image. (b) Dark-field image. (c) SAED pattern. (d) Higher magnification image. (e) SAED patterns of Zone A. (f) SAED patterns of Zone B. (g) SAED patterns of Zone C.

The SAED pattern in Fig. 4c of the entire thickness of the coating displays segments of the (111), (200), and (220) fcc diffraction rings. Three SAED patterns of equal size were labeled as Zones A, B, and C, as presented in Figs. 4e–g. Zone A had a broad diffused halo and was amorphous. Zone B contained arc-like fcc diffraction rings, implying a polycrystalline structure. Zone C revealed a large single-grain SAED with an fcc structure. An amorphous native Si oxide layer existed on the surfaces of the Si substrates, and an amorphous 270 nm-thick (TiVCrZrHf)N layer initiated near the substrate. Then, randomly oriented small (TiVCrZrHf)N grains formed above the amorphous structure, and thereafter tapered crystallites with an fcc crystal phase began to develop. Fig. 4d is a higher magnification image. Similar to the aforementioned SEM observations, a very dense and compact columnar structure without both inter- and intra-columnar voids was present. These results clearly indicated that the domain structure sharply varied with the film thickness, being primarily amorphous near the substrate and increasingly fcc crystal away from this interface. The microstructural evolution found was similar to that observed by Song and Liu et al. [34,35]. They have considered that the lattice mismatch between the coating and substrate is the main reason for the variation in the coating structure. However, there is no epitaxy in this case; this explanation is not even plausible and should not be mentioned. Some other dominant factors should be proposed. First, incorporating multi-elements with different atomic sizes induces lattice distortion and consequently limits the diffusion of atoms. Second, the residual stress (~6.3 GPa) and renucleation effect caused by the substrate bias promote the amorphization of the coating structure. Accordingly, the unusual transition from amorphous to polycrystalline structure occurs. Fig. 5 shows the cross-sectional TEM micrographs of the (TiVCrZrHf)N coating annealed at 400 °C. A surface oxide layer (~95 nm) with visible voids and pores formed on the coating (Figs. 3c, 5a–c), and its composition was identified by energy dispersive spectroscopy spot analysis. The SAED and nanobeam diffraction observations revealed that the surface oxide layer had an amorphous structure (Fig. 5d–f). There was no other significant change in the structure or composition. The formation of voids and pores may result from the nitrogen release and large volume expansion during the oxidation. Notably, the oxide layer adjacent to the nitride layer retained some nitride crystallites (Fig. 5g). The same phenomenon was also observed in the (TiVCrZrHf)N coating annealed at 500 °C (Fig. 6d), which indicated that the oxidation was diffusion controlled. Fig. 6 shows the cross-sectional

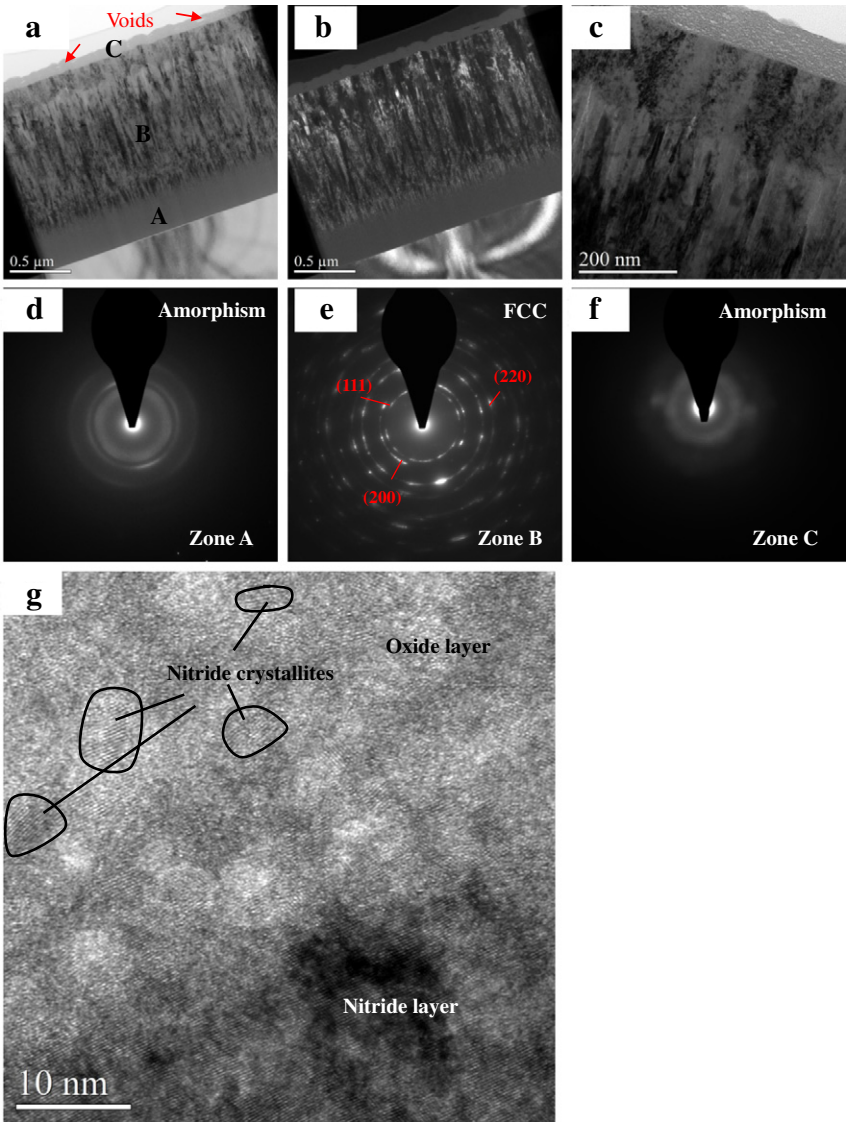

Fig. 5. Cross-sectional TEM micrographs of the as-deposited (TiVCrZrHf)N coatings after 400 °C in air. (a) Bright-field image. (b) Dark-field image. (c) Higher magnification image. (d) SAED patterns of Zone A. (e) SAED patterns of Zone B. (f) SAED patterns of Zone C. (g) High resolution TEM lattice image.

TEM micrographs of the 500 °C-annealed (TiVCrZrHf)N coating, whose surface oxide layer expectedly thickened to ~280 nm (Figs. 3d, 6a–d). Its structure became looser and more porous. Fig. 7 shows the cross-sectional TEM micrographs of the (TiVCrZrHf)N coating annealed at 600 °C. It was found that further increased annealing temperature to 600 °C yielded an almost fully developed oxide scale (~2800 nm) throughout the (TiVCrZrHf)N coatings, as shown in Figs. 3e and 7a. Apparently, a large number of voids and severely crack existed in the oxidation section of the coating. Two dominant factors are expected. First, the transformation from amorphous to crystallized oxide structure may be accompanied by extra volume increase that causes extensive voids. Second, the difference in the thermal expansion coefficient of the nitride and that of their oxide becomes significant when annealing at higher temperature. Thus, cracks parallel to the substrate are produced [36,37]. The SAED pattern displayed segments of the (011), (111), and (200) $ZrTiO_4$ diffraction rings (Zone A) (Fig. 7b). The primary diffracted intensity along the growth direction emanated from the 111-oriented grains, reflecting the (111) preferred orientation of the coating. The result was consistent with the XRD analysis. However, there were still 290 nm-thick amorphous structures within the oxide layer (Zone B) (Fig. 7c), indicating the insufficient diffusion reaction of oxygen. Noticeably, a 270 nm-thick amorphous nitride layer and 50 nm-thick randomly oriented nanocrystallites remained near the substrate (Zones C and D) because their structures annihilated the rapid oxidation paths along the grain boundaries (Fig. 7d and e). After high-temperature thermal annealing at 700 °C, the coating completely oxidized and its thickness was 3160 nm, as shown in Fig. 3f. The oxidation resistance performance of the (TiVCrZrHf)N coating was concluded in Fig. 8. In order to improve oxidation resistance, further research and development in the (TiVCrZrHf)N coatings would still be required.

Fig. 9 shows the variations in the hardness and elastic modulus of the (TiVCrZrHf)N coatings after annealing at different temperatures in air. The hardness of the as-deposited (TiVCrZrHf)N coating was about 31.24 GPa. Annealing at 300 °C caused no obvious change in hardness. However, the coating hardness softened to 21.91 GPa after annealing at 400 °C with the intervention of oxidation, especially on the surface. Annealing at 500 °C caused the hardness to drop further to 11.85 GPa. Annealing at above 600 °C caused the coatings to be completely oxidized, and the very low hardness of 2.3 GPa was obtained. Fig. 10 shows the variations in the electrical resistivity of the (TiVCrZrHf)N coatings after annealing at different temperatures in air. The electrical resistivity of the (TiVCrZrHf)N coatings

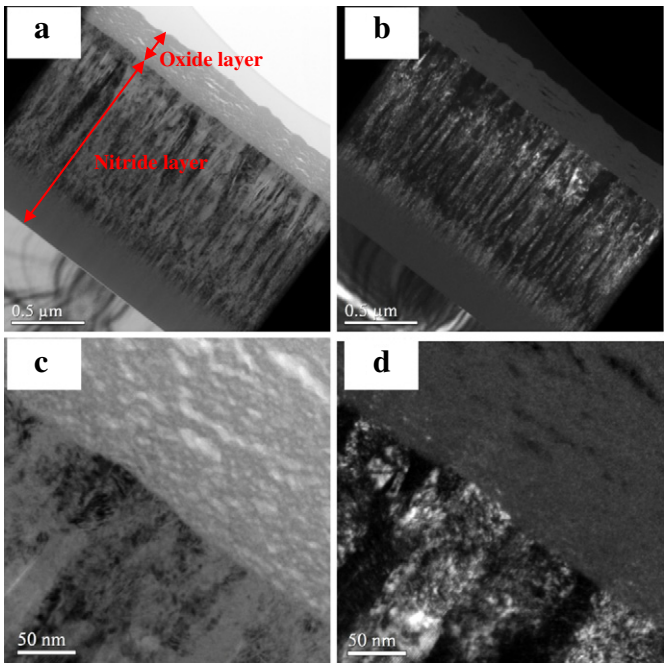

Fig. 6. Cross-sectional TEM micrographs of the as-deposited (TiVCrZrHf)N coatings after 500 °C in air. (a) Bright-field image. (b) Dark-field image. (c) Higher magnification bright-field image. (d) Higher magnification dark-field image.

was stable at a low level, similar to its as-deposited state of about 144 μΩ-cm, up to 300 °C. With increased annealing temperatures to 400 and 500 °C, with the evident emergence of the surface oxide layer, the electrical resistivity of the coatings significantly increased. The electrical resistivity further increased by six orders of magnitude or more due to the nearly completed oxidation when the annealing temperature was increased to 600 and 700 °C. These results indicated that oxidation detrimentally affected the mechanical and electrical properties of the nitride coatings. This trend is associated with the thicker surface oxide layer. In general, oxide has smaller values for the hardness and conductivity than nitride and thus the existence of surface oxide layer tends to lower the hardness down to values similar to the

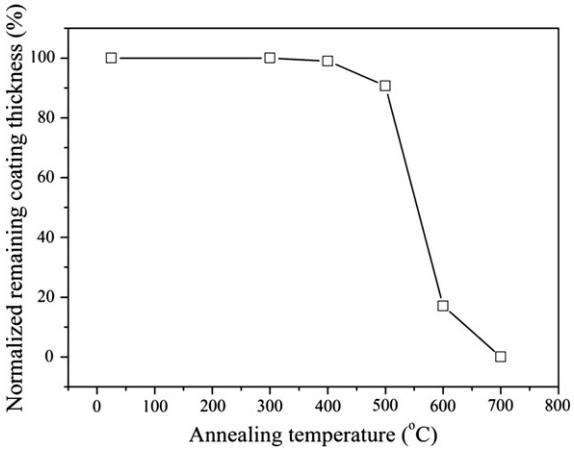

Fig. 8. The remaining unoxidized nitride thicknesses of (TiVCrZrHf)N, normalized to the initial coating thickness, as a function of annealing temperature in air.

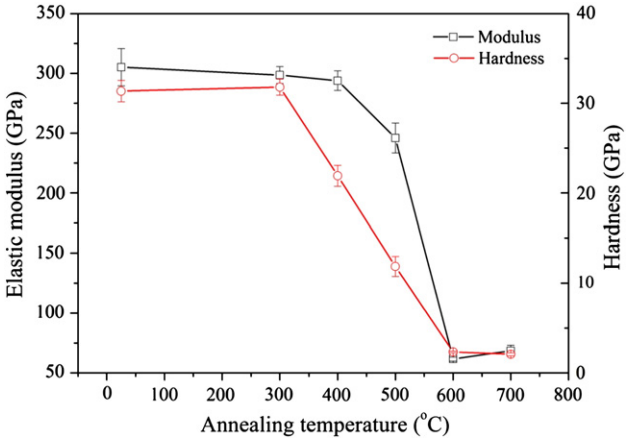

Fig. 9. Hardness and elastic modulus of the (TiVCrZrHf)N coatings after annealing at different temperatures in air.

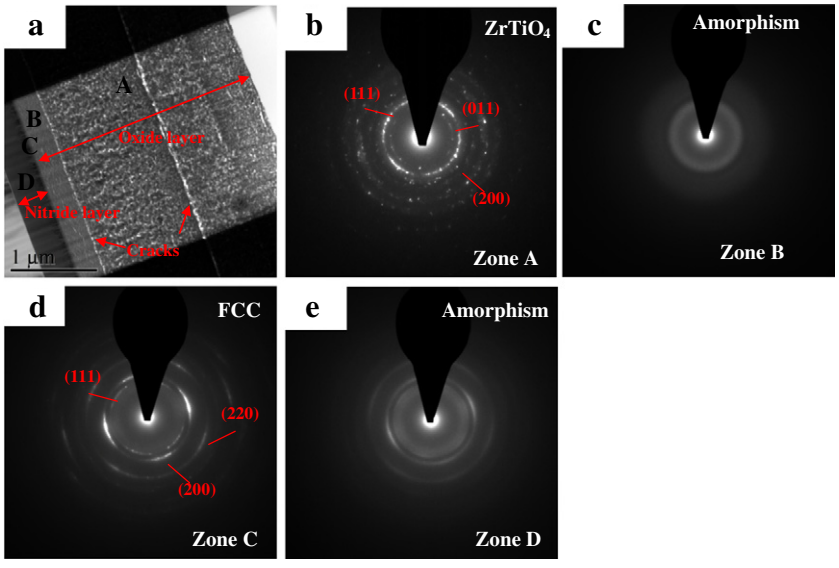

Fig. 7. Cross-sectional TEM micrographs of the as-deposited (TiVCrZrHf)N coatings after 600 °C in air. (a) Bright-field image. (b) SAED patterns of Zone A. (c) SAED patterns of Zone B. (d) SAED patterns of Zone C. (e) SAED patterns of Zone D.

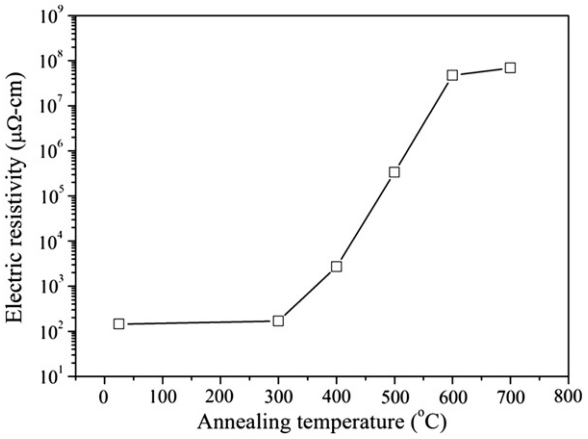

Fig. 10. Electric resistivity of the (TiVCrZrHf)N coatings after annealing at different temperatures in air.

oxide. Moreover, because the incorporated voids occupy the oxide layer volume without significant contribution to the mass, strength, and conductivity [38], the enhanced volume fraction of the voids with annealing temperature in air is expected to deteriorate the mechanical and electrical properties strongly.

4. Conclusions

Multi-component (TiVCrZrHf)N hard coatings were prepared by RF magnetron sputtering, and their temperature oxidation behavior was studied. TEM revealed that the as-deposited coatings had an amorphous structure in the initial sputtering period, but the fcc crystal phase started to grow with increased sputtering time, which may due to the severely distorted lattices and residual stress. In conjunction with EPMA, XRD, SEM, and TEM analyses, the coating started to oxidize at 400 °C and was almost fully oxidized at 600 °C. The oxide layer was amorphous and preferentially formed on the surface under 500 °C. With further increased temperature to 600 °C, a hexagonal $ZrTiO_4$ phase developed. Monoclinic ZrO_2 and rutile TiO_2 were observed with further increased temperature to 700 °C. The oxide layer thickened and loosened with visible voids and pores with increased annealing temperature. Accordingly, the physical properties of the coatings deteriorated due to the formation of an oxide layer with a loose structure. The hardness of (TiVCrZrHf)N decreased to 2.3 GPa and its electrical resistivity increased to 100 Ω-cm.

Acknowledgments

The authors gratefully acknowledge the financial support for this research by the National Science Council of Taiwan under grant no. NSC100-2221-E-005-034-MY3.

References

[1] L.E. Toth, Transition Metal Carbides and Nitrides, Academic, New York, 1971.
[2] Y. Xi, H. Fan, W. Liu, J. Alloys Compd. 496 (2010) 695.
[3] A. Kumar, D. Singh, R. Kumar, D. Kaur, J. Alloys Compd. 479 (2009) 166.
[4] J.L. Ruan, D.F. Lii, H.H. Lu, J.S. Chen, J.L. Huang, J. Alloys Compd. 478 (2009) 671.
[5] V.M. Vishnyakov, V.I. Bachurin, K.F. Minnebaev, R. Valizadeh, D.G. Teer, J.S. Colligon, V.V. Vishnyakov, V.E. Yurasova, Thin Solid Films 497 (2006) 189.
[6] S.M. Aouadi, K.C. Wong, K.A.R. Mitchell, F. Namavar, E. Tobin, D.M. Mihut, S.L. Rohde, Appl. Surf. Sci. 229 (2004) 387.
[7] M. Uchida, N. Nihira, A. Mitsuo, K. Toyoda, K. Kubota, T. Aizawa, Surf. Coat. Technol. 177–178 (2004) 627.
[8] H. Hasegawa, A. Kimura, T. Suzuki, J. Vac. Sci. Technol. A 18 (2000) 1038.
[9] U. Helmersson, S. Todorova, S.A. Barnett, J.E. Sundgren, L.C. Markert, J.E. Greene, J. Appl. Phys. 62 (1987) 481.
[10] M. Shinn, L. Hultman, S.A. Barnett, J. Mater. Res. 7 (1992) 901.
[11] S. Vepřek, Thin Solid Films 317 (1998) 449.
[12] S. Vepřek, P. Nesládek, A. Niederhofer, F. Glatz, M. Jílek, M. Šíma, Surf. Coat. Technol. 108–109 (1998) 138.
[13] J.W. Yeh, S.K. Chen, S.J. Lin, J.Y. Gan, T.S. Chin, T.T. Shun, C.H. Tsau, S.Y. Chang, Adv. Eng. Mater. 6 (2004) 299.
[14] P.K. Huang, J.W. Yeh, T.T. Shun, S.K. Chen, Adv. Eng. Mater. 6 (2004) 74.
[15] C.J. Tong, M.R. Chen, S.K. Chen, J.W. Yeh, T.T. Shun, S.J. Lin, S.Y. Chang, Metall. Mater. Trans. A36 (2005) 1263.
[16] Y.J. Zhou, Y. Zhang, Y.L. Wang, G.L. Chen, Mater. Sci. Eng. A454–455 (2007) 260.
[17] M.R. Chen, S.J. Lin, J.W. Yeh, S.K. Chen, Y.S. Huang, M.H. Chuang, Metall. Mater. Trans. A37 (2006) 1363.
[18] B.S. Li, Y.P. Wang, M.X. Ren, C. Yang, H.Z. Fu, Mater. Sci. Eng., A 498 (2008) 482.
[19] D.C. Tsai, Y.L. Huang, S.R. Lin, S.C. Liang, F.S. Shieu, Appl. Surf. Sci. 257 (2010) 1361.
[20] S.C. Liang, Z.C. Chang, D.C. Tsai, Y.C. Lin, H.S. Sung, M.J. Deng, F.S. Shieu, Appl. Surf. Sci. 257 (2011) 7709.
[21] S.C. Liang, D.C. Tsai, Z.C. Chang, H.S. Sung, Y.C. Lin, Y.J. Yeh, M.J. Deng, F.S. Shieu, Appl. Surf. Sci. 258 (2011) 399.
[22] D.C. Tsai, S.C. Liang, Z.C. Chang, T.N. Lin, M.H. Shiao, F.S. Shieu, Surf. Coat. Technol. 207 (2012) 293.
[23] S.Y. Chang, S.Y. Lin, Y.C. Huang, C.L. Wu, Surf. Coat. Technol. 204 (2010) 3307.
[24] P.K. Huang, J.W. Yeh, Surf. Coat. Technol. 203 (2009) 1891.
[25] S.C. Liang, D.C. Tsai, Z.C. Chang, T.N. Lin, M.H. Shiao, F.S. Shieu, Electrochem. Solid-State Lett. 15 (2012) H5.
[26] H.O. Pierson, Handbook of Refractory Carbides and Nitrides, Noyes Publications, Westwood, New Jersey, 1996.
[27] J.A. Dean, Lange's Handbook of Chemistry, McGraw-Hill, 1999.
[28] D.C. Tsai, Y.L. Huang, S.R. Lin, D.R. Jung, S.Y. Chang, F.S. Shieu, J. Alloys Compd. 509 (2011) 3141.
[29] C.H. Kim, M. Lee, Bull. Korean Chem. Soc. 23 (2002) 741.
[30] B.M. Reddy, B. Chowdhury, J. Catal. 179 (1998) 413.
[31] T. Noguchi, M. Mizuno, Sol. Energy 11 (1967) 56.
[32] J.C. Wu, S.C. Chung, A.Y. Ching-Lan, I. Wang, J. Catal. 87 (1984) 98.
[33] I.C. Cosentino, E.N.S. Muccillo, R. Muccillo, F.M. Vichi, Sol–Gel. Sci. Technol. 37 (2006) 31.
[34] J.H. Song, S.C. Wang, J.C. Sung, J.L. Huang, D.F. Lii, Thin Solid Films 517 (2009) 4753.
[35] W.J. Liu, S.J. Wu, C.M. Chen, Y.C. Lai, C.H. Chuang, J. Cryst. Growth 276 (2005) 525.
[36] D. McIntyre, J.E. Greene, G. Håkansson, J.E. Sundgren, W.D. Münz, J. Appl. Phys. 67 (1990) 1542.
[37] Y.H. Koh, J.J. Choi, H.E. Kim, J. Am. Ceram. Soc. 83 (2000) 306.
[38] D.C. Tsai, F.S. Shieu, S.Y. Chang, H.C. Yao, M.J. Deng, J. Electrochem. Soc. 157 (2010) K52.